

Optimizing Raman quantum memory with dynamic phase

Sheng MING¹, Jinxian GUO^{1,2*}, Yuan WU³, Guzhi BAO^{1,2}, Shuhe WU^{1,2},
Minwei SHI^{1,2}, Liqing CHEN^{2,3} & Weiping ZHANG^{1,2,4,5*}

¹*School of Physics and Astronomy, and Tsung-Dao Lee Institute, Shanghai Jiao Tong University, Shanghai 200240, China;*

²*Shanghai Research Center for Quantum Sciences, Shanghai 201315, China;*

³*State Key Laboratory of Precision Spectroscopy, Quantum Institute of Atom and Light, Department of Physics, East China Normal University, Shanghai 200062, China;*

⁴*Collaborative Innovation Center of Extreme Optics, Shanxi University, Taiyuan 030006, China;*

⁵*Shanghai Branch, Hefei National Laboratory, Shanghai 201315, China*

Received 5 September 2022/Revised 29 September 2022/Accepted 28 October 2022/Published online 19 June 2023

Abstract Optical quantum memory is a key component of emerging quantum technologies and applications. One of the most promising protocols, far-off-resonant Raman memory, is still beset by its efficiency. Until now, the only effective method for enhancing its efficiency in experiments has been the intensity modulation method on the control field, while the experimental demonstrations still fail to meet the theoretical expectation. In this study, we experimentally demonstrate how to optimize the Raman quantum memory process using a new method called phase modulation; 52.7% total memory efficiency is realized by applying a phase modulation on the control field with a near-square intensity waveform of the control field, thereby resulting in an increase in efficiency of 13.3% compared to the best case of no phase modulation. Additionally, a hybrid method, combining the phase and intensity modulations, is demonstrated with 87.3% memory efficiency. Such high-efficiency results in 99.0% unconditional fidelity even at near single photon level. The unconditional fidelity is always higher than that of the intensity method as the input photon number of the signal increases and can still beat the nonclone limit, even at 128.1 photons/pulse. Our phase modulation method has great potential applications in quantum information processing due to the advantages of low experimental requirements but an additional degree of freedom and high performance, especially for the high speed and high photon number state manipulation.

Keywords quantum information, quantum optics, quantum communication, quantum memory, Raman scattering

Citation Ming S, Guo J X, Wu Y, et al. Optimizing Raman quantum memory with dynamic phase. *Sci China Inf Sci*, 2023, 66(8): 180505, <https://doi.org/10.1007/s11432-022-3614-7>

1 Introduction

Quantum memory is an important component in various quantum technologies, including optical quantum state generation [1], quantum communication [2], and linear-optical quantum computing [3]. Several approaches, including far off-resonant Raman memory [4,5], gradient photon echo [6,7], electromagnetically induced transparency [8–10] (EIT), and atomic frequency comb [11,12] (AFC), have been demonstrated in various media, including hot atomic vapors [13], cold atomic ensembles [14], and solids doped with rare earth ions [15]. The goal of these approaches is to write an incoming signal pulse into an atomic spin wave and recover as much of it back as possible, which requires high efficiency and fidelity.

Far-off-resonant Raman memory is predominant among the quantum memory protocols for storing short signal pulses. Especially, true-single photon memory using Raman-type protocol was first realized [16] in 2015. Furthermore, high efficiency and fidelity [5], multimode [17], and THz-bandwidth memories [18] have been demonstrated recently. However, its use is still hampered by its efficiency and

* Corresponding author (email: jxguo@sjtu.edu.cn, wpz@sjtu.edu.cn)

unconditional fidelity. Until now, the only effective way to achieve high performance of Raman memory in experiments is the intensity modulation method [19], while the experimental demonstrations have failed to meet the theoretical expectations. This is due to the imperfect intensity waveform modulation in the experiments and the time-varying AC Stark shift caused by the high control pulse power.

To avoid these problems, several optimization methods, including frequency chirps [20, 21], spatial phase-matching [20, 22–24], and refractive index manipulation [25, 26] methods, are proposed to replace the intensity modulation method. These methods take advantage of the phase-matching condition in the memory process, but no further efficiency improvement is achieved in experiments, thereby limiting their unconditional fidelity. Instead of replacing the intensity modulation method, a simple phase control method that can be combined with the intensity method to overcome its problems and further improve efficiency and fidelity should be investigated.

A phase modulation method based on dynamically manipulating the two-photon detuning was investigated in this work. The experimental demonstration shows that even with a near-square intensity waveform of control light, 52.7% total efficiency can still be achieved by simply adjusting the phase dynamically. In comparison to the case without phase modulation, our phase modulation method increases the efficiency by 13.3%. Furthermore, the phase modulation can be combined with the intensity modulation to achieve 87.3% total efficiency, corresponding to a 4.0% absolute increase in efficiency over the best efficiency achieved with only the intensity modulation. Even with near single photon-level input, the total efficiency is maintained at 87.3% with unconditional fidelity reaching 99.0%. Even if the photon number of the input state is up to 128.1 photons/pulse, the unconditional fidelity of our method can outperform the nonclone limit. In comparison to the intensity method, which can only beat the nonclone limit of 89.6 photons/pulse, there is nearly 42.9% improvement in the photon number.

2 Theoretical model

Considering a Raman quantum memory with phase modulation operated in a Λ -type atomic ensemble, an input signal with single photon detuning Δ_s is mapped into (in storage process) and out (in retrieval process) of the ensemble by a control field with time-varying detuning $\Delta_c(t)$ and effective Rabi frequency $\Omega(t)$. To simplify the discussion of temporal control in the memory process, the propagation effect is neglected and only the evolution of the total signal field and spin wave in the ensemble is considered. In this way, the memory process can be treated as an input-output response coupling system which gives clear physics of the dynamic phase manipulation method. We integrate the equations in [19] along z direction (see Appendix A) with the large detuning assumption $\Delta_s \gg \gamma, |\Omega(t)|$, where γ is the decay rate of the excited state $|e\rangle$. Then the evolution equation becomes

$$\frac{d}{dt}\hat{\Psi} = H_{\text{eff}}\hat{\Psi} + \hat{\Psi}_{\text{in-out}}, \quad (1)$$

where $\hat{\Psi} = [\hat{A}(t), \hat{B}(t)]^T$ is the operator inside the ensemble which consists of the integrated total signal field $\hat{A}(t)$ and atomic spin wave $\hat{B}(t)$. The input-output operators $\hat{\Psi}_{\text{in-out}} = [\hat{E}_{\text{in}}(t) - \hat{E}_{\text{out}}(t), 0]^T$ consist of the input signal $\hat{E}_{\text{in}}(t)$ at position $z = 0$, the output signal $\hat{E}_{\text{out}}(t)$ at $z = L$. The explicit expression of $\hat{E}_{\text{out}}(t)$ is given in Appendix B. Even if $\hat{E}_{\text{out}}(t)$ depends on $\hat{E}_{\text{in}}(t)$, the influence of $\hat{E}_{\text{out}}(t)$ can be ignored when optimizing the write process because in most cases $\hat{E}_{\text{out}}(t) \ll \hat{E}_{\text{in}}(t)$. The effective Hamiltonian which describes the coupling between atomic spin wave and signal field is

$$H_{\text{eff}} = i \begin{pmatrix} 0 & \tilde{\kappa}(t) \\ \tilde{\kappa}^*(t) & -\tilde{\delta}(t) \end{pmatrix}, \quad (2)$$

where $\tilde{\kappa}(t) = g\sqrt{N}\Omega(t)/\Delta_s$ is the transform coefficient with the atom-field coupling constant g , the atomic number N , and the time-varying Rabi frequency of the control field $\Omega(t)$. The two-photon detuning $\tilde{\delta}(t) = \delta_c(t) - |\Omega(t)|^2/\Delta_s$ consists of two parts, time-dependent frequency difference $\delta_c(t) = \Delta_c(t) - \Delta_s$ and the AC Stark shift term $|\Omega(t)|^2/\Delta_s$.

Then the solution of (1) can be obtained as follows:

$$\hat{\Psi} = U^\dagger(t, 0) \int_0^t U(t', 0) \hat{\Psi}_{\text{in-out}}(t') dt', \quad (3)$$

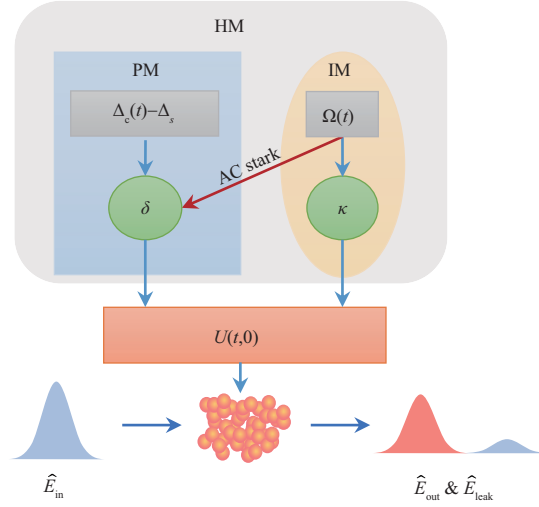


Figure 1 (Color online) Theoretical scheme to optimize Raman quantum memory with phase modulation (PM), intensity modulation (IM), and hybrid modulation (HM). The memory process is determined by transform coefficient κ and two-photon detuning δ through the propagator $U(t, 0)$. The IM method controls κ through a time-varying Rabi frequency $\Omega(t)$ but induces an AC Stark shift on δ . While the PM method only controls delta and the HM method controls both δ and κ .

where $U(t, 0) = \exp(-\int_0^t H_{\text{eff}}(t') dt')$ is a propagator, which describes the response of the memory system. As shown in Figure 1, the propagator $U(t, 0)$ converts the input signal into the output signal and determines the evolution of the signal field and atomic spin wave inside the ensemble. The propagator is rearranged and divided into two parts to optimize the memory process,

$$U(t, 0) = \left[\begin{array}{cc} \cos \phi - i \cos \theta \sin \phi & 0 \\ 0 & \cos \phi + i \cos \theta \sin \phi \end{array} \right] - i \left[\begin{array}{cc} 0 & \sin \theta \\ \sin \theta^* & 0 \end{array} \right] \sin \phi \Big] e^{i\frac{\delta}{2}}, \quad (4)$$

where $\phi = \sqrt{\delta^2 + 4|\kappa|^2}/2$, $\cos \theta = \delta/\sqrt{\delta^2 + 4|\kappa|^2}$, $\delta(t) = \int_0^t \tilde{\delta}(t') dt'$, and $\kappa(t) = \int_0^t \tilde{\kappa}(t') dt'$.

As we can see in (4), the matrix with diagonal elements represents the independent evolution of the signal field and atomic spin wave, while the matrix with anti-diagonal elements describes the conversion between them. The anti-diagonal elements should be well adjusted to achieve a perfect quantum memory process, especially a perfect write process [21, 27]. At the beginning of the memory process, the anti-diagonal elements $\sin \phi$ and $\sin \theta$ should be as large as possible to obtain a strong conversion between the signal light and atomic spin wave. Then the elements should be adiabatically tuned to zero to keep the lights stored in the spin wave. Such control can be achieved by a time-varying two-photon detuning δ or coupling coefficient κ according to (4) since both $\sin \phi$ and $\sin \theta$ are dependent on them. This is the basis of both phase and intensity modulation methods. For example, the traditional intensity modulation method (shown in Figure 1) controls $\kappa(t)$ through a time-varying Rabi frequency $\Omega(t)$. However, the inevitable AC Stark shift causes a non-zero two-photon detuning $\delta(t)$, making $\sin \theta < 1$, which weakens the coupling between light and atoms.

We dynamically modulate the phase of the control field δ_c to realize a time-varying two-photon detuning δ in our phase modulation method, as shown in Figure 1. To keep the light interacting with the atomic spin wave, a non-zero κ is maintained in our method. Then a strong coupling can be achieved by a small two-photon detuning, $\delta \ll |\kappa|$. The detuning should satisfy $\delta \gg |\kappa|$ or $\phi \approx \pi$ to shut down the coupling, which makes $\sin \theta \approx 0$ or $\sin \phi \approx 0$, respectively. Therefore, the optimization of efficiency can be achieved by temporally adjusting the two-photon detuning from $\delta \ll |\kappa|$ to $\delta \gg |\kappa|$. However, the optimal condition of the temporal phase waveform is quite complicated due to the highly nonlinear relations in (4). Benefiting from the development of optimal control, we can automatically search the optimal condition of phase waveform online by algorithms as in the intensity modulation method [28].

Interesting thing is, the propagator in (4) depends on not only δ but also κ , which means that the intensity modulation method and our phase modulation method can be combined. Such a hybrid mod-

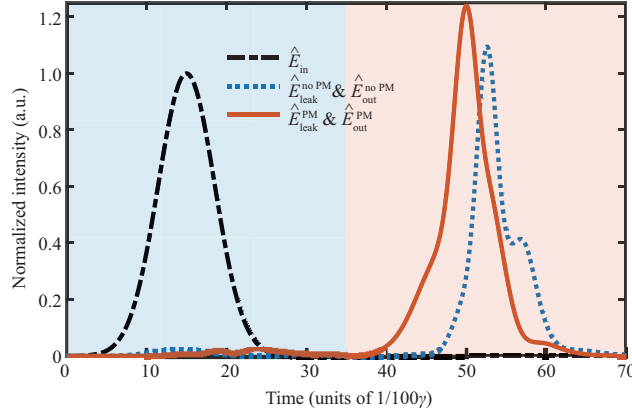


Figure 2 (Color online) Theoretical waveforms of the incoming signal \hat{E}_{in} (black dash-dotted line), leakage signal with intensity modulation (blue dotted line), and dynamic phase modulation \hat{E}_{leak}^{PM} (red solid line). Correspondingly, the readout signals are shown in the right panel.

ulation method can effectively improve the degree of freedom of the optimization and make it easier to achieve a high-performance quantum memory process. A perfect intensity waveform matching by only applying the intensity modulation method is not so easy to realize in experiments, especially when storing fast or high-order temporal mode signals. For example, an imperfect intensity waveform (such as Gaussian pulse [28]) is applied to store a signal (the black dash-dotted line in Figure 2). The simulation only shows 68.2% memory efficiency (the blue dotted line in Figure 2). With hybrid modulation, a time-varying phase is applied to such an imperfect intensity waveform which can further improve the memory efficiency. Combining with a dynamical phase, the final efficiency increases to 95.1% (the red solid line in Figure 2). Therefore, our phase modulation method is an effective way to achieve high efficiency.

3 Experimental setup

A Raman memory apparatus is set up to experimentally demonstrate the phase modulation method. The atomic energy level scheme and experimental setup are shown in Figure 3. A 7.5 cm-long cell with the diameter of 2.5 cm filled with ^{87}Rb atoms is heated to 75°C. The cell is coated with paraffin to mitigate decoherence induced by collisions between cell walls and rubidium atoms. A four-layer permalloy magnetic shield surrounds the cell to reduce spin decoherence caused by remnant magnetic fields. The atoms are initially prepared in the upper hyperfine level of the ground state of ^{87}Rb , $|g\rangle = |5S_{1/2}, F = 2\rangle$, by a 45- μs -long optical pumping pulse at the wavelength of 780 nm. Then an incoming signal pulse \hat{E}_{in} at the wavelength of 795 nm is mapped into atomic spin wave \hat{B} by the strong write pulse W , where \hat{E}_{in} is horizontally polarized and blue-detuned by 2.5 GHz from the transition $|g\rangle \rightarrow |e\rangle = |5P_{1/2}\rangle$ while the write pulse W is vertically polarized and blue-detuned by 2.5 GHz from the transition $|m\rangle = |5S_{1/2}, F = 1\rangle \rightarrow |e\rangle$. These two beams come from two semiconductor lasers (Toptica, DLPros) and are phase locked [29] with a frequency difference of 6.834 GHz, the energy level splitting between $|g\rangle$ and $|m\rangle$.

Phase modulation on write beam W should be conducted to optimize the efficiency. The write beam passes through a fiber electro-optic modulator (EOM) with a low damage threshold to experience the phase modulation (PM) process before being amplified by the tapered amplifier (TA, Boosta). The EOM is controlled by an arbitrary waveform generator (AWG) whose voltage varies from -1 to 1 V, corresponding to the phase from $-\pi/4$ to $\pi/4$. The temporal intensity waveforms of both beams are independently controlled by acousto-optic modulators (AOMs) with rising edge time of 22 and 30 ns, respectively. After those AOMs, the write pulse and incoming signal pulse are spatially overlapped by a Glan polarizer before the atomic cell. The beam diameters in the cell are 600 and 350 μm for the write pulse and the incoming signal, respectively. Correspondingly, the atoms involved in the memory process are approximate 2.5×10^{10} . After the cell, the leaking signal pulse can be separated from the strong write pulse by another Glan polarizer with an extinction ratio of 40 dB. The separated signal pulse is frequency filtered by an etalon whose transmission frequency is the same as the signal field before intensity detection. The transmission of the etalon is 80% and the finesse is about 400.

After the write process, a read pulse R at the wavelength of 795 nm with a duration of 300 ns, coming

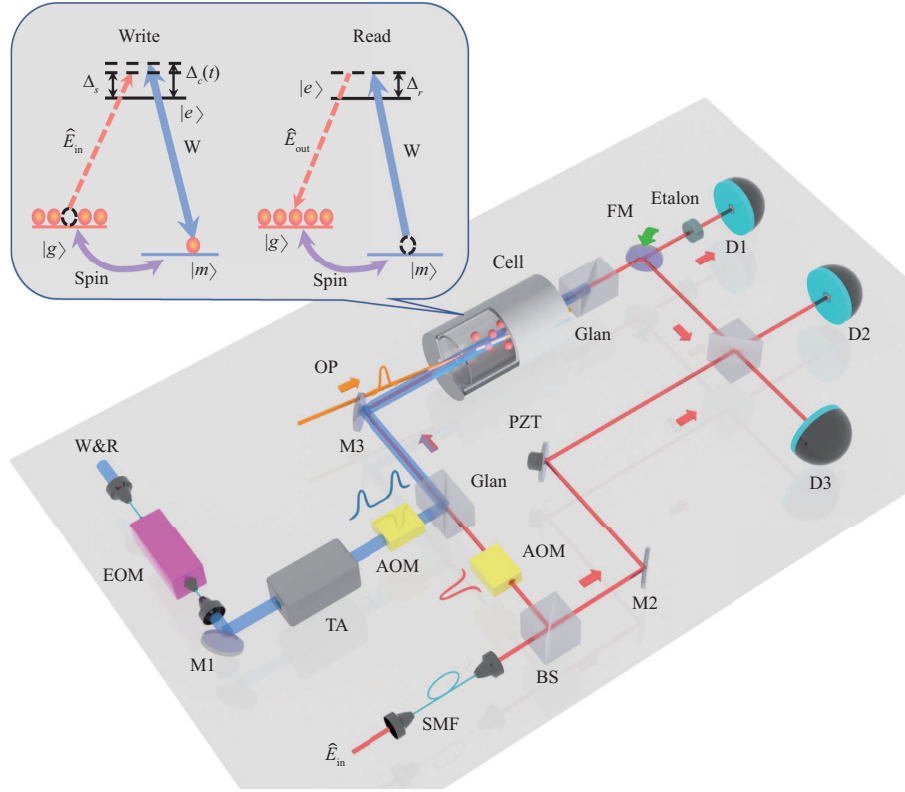


Figure 3 (Color online) Experimental setup and energy levels for Raman memory. $|g, m\rangle$: hyperfine levels $|5S_{1/2}, F = 2, 1\rangle$, $|e\rangle$: excited state $|5P_{1/2}\rangle$. W : write field, R : read field, \hat{E}_{in} : input signal, \hat{E}_{out} : readout signal, $\Delta_c(t)$: single photon detuning of write field, Δ_r : single photon detuning of read field. OP: optical pumping, EOM: electro-optic modulator, AOM: acousto-optic modulator, TA: tapered amplifier, SMF: single mode fiber, PZT: piezo transducer, FM: folding mirror, M1–M3: mirrors, D1–D3: detectors.

from the same laser as the write pulse but without phase modulation, is sent into the atomic ensemble to read the spin wave \hat{B} into the output signal light. The readout signal is separated from the read pulse by Glan polarizer and etalon after the cell and detected with intensity detector D1. To evaluate the fidelity at the single photon level, the homodyne detection with optical tomography is used to obtain the density matrix of input and readout signals.

4 Results

4.1 Phase modulation method

As shown in Figure 4(a), a Gaussian-shaped signal pulse with full width at half maximum (FWHM) of 26 ns (the black dash-dotted line) is coherently mapped into the atomic spin wave with a nearly square-shaped write pulse shown as the dashed purple line. As discussed in the theoretical model, a temporal phase waveform is applied to the write field through the EOM to realize the optimization of the memory process. We use an iteration optimization procedure based on differential evolution algorithm [30] with global search ability and rapid convergence to optimize the phase waveform of the write field. The algorithm takes the total efficiency as the criteria of phase waveform which is defined by

$$\eta = N_{\hat{E}_{out}} / N_{\hat{E}_{in}}, \quad (5)$$

where $N_{\hat{E}_{out}}$ and $N_{\hat{E}_{in}}$ are the photon numbers of the readout signal in the read process and the incoming signal in the write process, respectively. The phase waveform in our experiment consists of a set of voltages applied to the EOM. The set of voltages is equally spaced in time during the storage process, output from AWG to the EOM.

The algorithm starts with a set of initial phase waveforms with randomly generated voltages, which we call individuals. In our experiment, 10 individuals are used to balance the convergence rate and

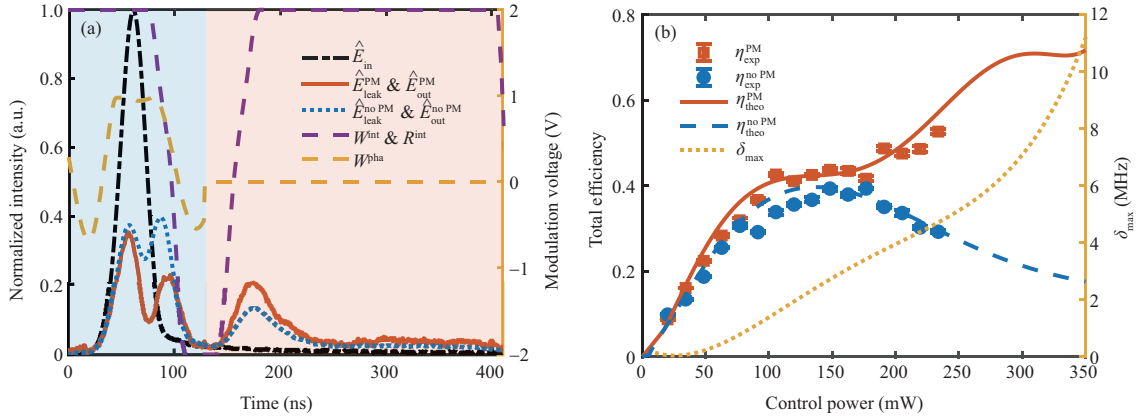


Figure 4 (Color online) (a) Waveforms of the incoming signal \hat{E}_{in}^{PM} (black dash-dotted line), leakage signal with phase modulation \hat{E}_{leak}^{PM} (red solid line) and without phase modulation $\hat{E}_{leak}^{no PM}$ (blue dotted line), near-square write pulse W^{int} (purple dashed line) with 32 ns falling edge limited by the AOM and the optimal phase waveform W^{pha} (yellow dashed line). Correspondingly, the readout signal with phase modulation \hat{E}_{out}^{PM} (red solid line) and without phase modulation $\hat{E}_{out}^{no PM}$ (blue dotted line) by the read pulse R^{int} (purple dashed line). (b) Total efficiency with phase method η^{PM} (red squares) and without phase modulation $\eta^{no PM}$ (blue circles) against the power of control pulse with the corresponding theoretical simulations (red solid line and blue dashed line). The yellow dotted line is the maximum difference of the effective two-photon detuning δ_{max} during the storage process.

accuracy of the algorithm. Each individual can correspondingly obtain an efficiency. These individuals experience mutation and crossover operations [31] to generate a new set of individuals with corresponding efficiencies. Then the algorithm compares the efficiencies of the two sets of individuals and keeps those individuals with higher efficiencies. Repeat these steps iteratively until no higher efficiency appears, i.e., the algorithm converges, which gives us an optimal phase waveform and the corresponding best efficiency. The whole procedure usually takes 3–4 min which corresponds to 10–15 iterations in our experiments.

The optimal phase waveform is obtained as the yellow dashed line shown in Figure 4(a) after applying the algorithm-assisted optimization. The corresponding readout signal after the cell (the red solid line in Figure 4(a)) indicates optimized total efficiency $\eta = 52.7\%$. As a comparison, the leakage and readout signal without phase modulation (the blue dotted line in Figure 4(a)) are also measured. The corresponding total efficiency is only 39.4%, representing that the phase modulation results in an increase in efficiency of 13.3%.

We plot the relation between η and the power of write light for square-shaped control in Figure 4(b) to further investigate the performance of the phase modulation method. η with and without phase modulation are nearly the same and increase rapidly before the power reaches 150 mW, which means our phase modulation method brings no significant improvement in the region of low control power. In this region, the control pulse of low power and poor intensity waveform matching lead to weak coupling between the signal and atomic spin wave. To further improve the efficiency, the phase modulation method should adjust δ to ensure both strong coupling and elimination of the intensity waveform mismatch effect. However, a small δ modulated by the phase modulation ensures a strong coupling but cannot eliminate the effect of intensity waveform mismatch. While a large δ can eliminate the effect of intensity waveform mismatch but it also weakens the atom-light coupling. The tradeoff between these two effects leads to the fact that phase modulation yields no significant improvement in efficiency.

The situation changes when the power keeps increasing to the high power region (>150 mW). The efficiency increases fast with power in the phase modulation case while the large power leads to a fast drop in efficiency in the no phase modulation case. Moreover, the corresponding theoretical simulation (the red solid line in the phase modulation case and the blue dashed line in no phase modulation case) shows this difference gets bigger when the power is higher. Furthermore, the efficiency can reach 71.7% at 300 mW with theoretical simulation in our phase modulation method. This is because the control pulse of high power ensures a strong atom-light coupling when dynamical phase modulation eliminates the effect of intensity waveform mismatch.

We define the maximum difference of the effective two-photon detuning δ_{max} in optimization to further prove the tradeoff effect. A small δ_{max} means a small two-photon detuning while the large δ_{max} means a large two-photon detuning when optimizing the memory process. As shown by the yellow dotted line in Figure 4(b), δ_{max} keeps small in the low power region but increases fast with power. In the high power region, δ_{max} is much larger than the one in the low power region. So tradeoff effect plays a more

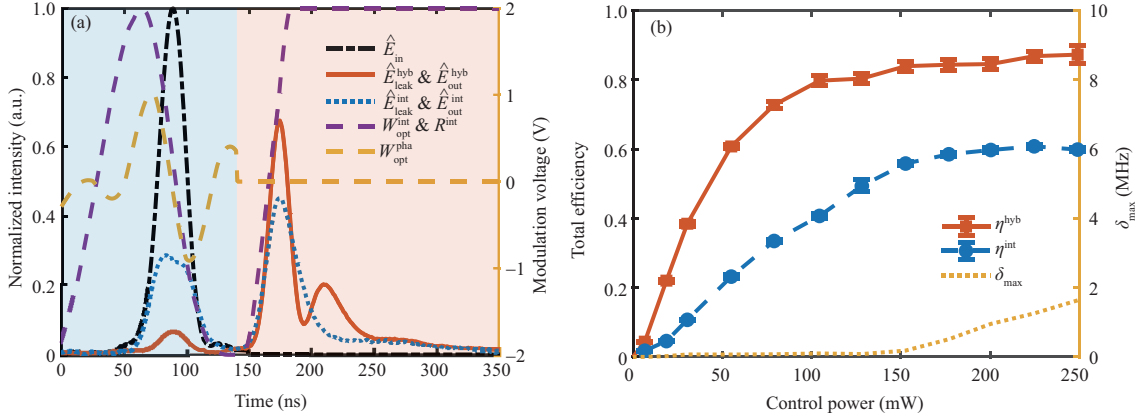


Figure 5 (Color online) (a) Waveforms of the incoming signal \hat{E}_{in} (black dash-dotted line), leakage signal with hybrid method \hat{E}_{leak}^{hyb} (red solid line) and with intensity method \hat{E}_{leak}^{int} (blue dotted line), the optimal write pulse W_{opt}^{int} (purple dashed line), and the optimal phase waveform W_{opt}^{pha} (yellow dashed line). Correspondingly, the readout signals with hybrid method \hat{E}_{out}^{hyb} (red solid line) and intensity modulation \hat{E}_{out}^{int} (blue dotted line) by the read pulse R^{int} (purple dashed line) are shown in the right panel. (b) Total memory efficiency η with hybrid method (red squares) and intensity method (blue circles) against the power of write light. The yellow dotted line is the maximum difference of the effective two-photon detuning δ_{max} during the storage process.

important role in the low-power region than in the high-power region.

4.2 Hybrid modulation method

Although the phase modulation method is effective, its efficiency could be further improved. The hybrid modulation method, which combines the phase and intensity modulation methods, is one possible way, as analyzed in our theoretical model. Generally, the combination is achieved by simultaneously applying an intensity modulation and phase modulation on the write light. We perform the two optimizations sequentially to avoid the experimental complexities of hybrid modulation. First, the intensity of the write pulse is optimized using a Gaussian optimization method proposed by Shinbrough et al. [28], which is an approximate solution for most of the optimal memory operations. Then, the phase of the write field is dynamically controlled to correct the imperfect intensity waveform matching.

When optimizing the intensity waveform, we use the same iteration optimization procedure described in Subsection 4.1 with some minor adjustments. The procedure begins with the same algorithm but with different individuals, which are a set of Gaussian write pulses with a randomly initialized temporal delay $\Delta\tau^W$ of the write pulse, relative to the signal field and its duration τ_{FWHM}^W . Using efficiency as the criterion, the algorithm iterates until it converges, which results in an optimal Gaussian intensity waveform and the corresponding efficiency. The phase modulation optimization procedure starts with the optimal Gaussian intensity waveform after the intensity waveform optimization is completed. Then, the optimal Gaussian intensity and corresponding phase waveforms with optimized efficiency are obtained using this hybrid method. Here, we only optimized the intensity and phase once since subsequent intensity and phase optimization yielded little improvement.

As shown in Figure 5(a), the same Gaussian-shaped signal pulse (black dashed-dotted line) as in the pure phase modulation case is used in the hybrid method. After optimization, the optimal waveforms of intensity and phase modulation are obtained and plotted in Figure 5(a). With only intensity modulation, the optimal intensity waveform (purple dashed line in Figure 5(a)) is a Gaussian pulse with its falling edge covering the entire signal pulse, which is consistent with [28]. However, the corresponding efficiency is only 59.8%. Then, additional phase modulation is applied, which generates an optimal phase waveform (yellow dashed line). The optimized readout signal (red solid line in Figure 5(a)) in the hybrid method has been greatly improved compared to the only intensity modulation case (blue dotted line in Figure 5(a)). The final efficiency is 87.3%, demonstrating that the hybrid method can further improve memory efficiency.

Similarly, the relationship between the power of the write light and the efficiency η of the pure intensity and hybrid modulation methods is shown in Figure 5(b). As the power of the write light increases, η increases rapidly to 60.8% at 200 mW with only the intensity modulation. Then, increasing the power causes a small decrease in η , which is very similar to the near-square write pulse case in Subsection 4.1. While in the hybrid modulation case, efficiency saturates at the point of 150 mW and remains at 87.3% as the power increases. Moreover, the additional phase modulation in the hybrid case can always achieve

higher efficiency than the pure intensity modulation case. In comparison to the pure intensity modulation and the pure phase modulation cases, the hybrid method achieves the best efficiency using the lowest power of write light.

Notably, the phase modulation can significantly improve the efficiency when the intensity waveform is well adjusted, regardless of how powerful the write light is. This is in contrast to the near-square write pulse case in Subsection 4.1, where significant improvement appears only in the high-power region. This is because the hybrid method achieves better intensity waveform matching than the near-square control pulse case. The better the intensity of waveform matching, the smaller the δ required to eliminate the effect of imperfect waveform mismatch. Thus, we can ignore the influence of the tradeoff effect when performing phase optimization with the hybrid method, as evidenced by the not-so-large δ_{\max} , as shown by the yellow dotted line in Figure 5(b). This is one of the reasons why the hybrid method is so efficient.

Another reason for the high efficiency is the suppression of the large dynamic AC Stark shift induced by the write field. To show the effect of the AC Stark shift term, we scan the two-photon detuning spectrum by manually changing the locking frequency between the signal and write light, which adds stationary two-photon detuning δ_0 by $\delta_c = \delta_0 + \Delta_c - \Delta_s$. Here, we set the null point of stationary two-photon detuning δ_0 as the locking frequency, equal to 6.834 GHz. The solid red line in Figure 6 shows that the maximum efficiency η reaches 87.3% with our hybrid method, appearing at the null point of stationary two-photon detuning $\delta_0 = 0$. The FWHM of the two-photon spectrum of η with the hybrid method is 29 MHz. In comparison, the FWHM of the two-photon spectrum of η of the pure intensity modulation case is only 25 MHz, which is smaller than that of our hybrid method. In our experiment, the total efficiency of the pure intensity modulation case can only reach 59.8% when $\delta_0 = 0$. Therefore, our dynamic phase modulation eliminates the dynamic AC Stark shift, which can help improve efficiency.

Traditionally, a rough way to compensate for the AC Stark shift is by locking the stationary two-photon detuning at specific frequencies [5]. As the blue line in Figure 6 shows, by scanning the stationary double photon detuning after the phase modulation, the maximum efficiency can reach 83.3% when $\delta_0 = -9$ MHz, but this is still 4.0% lower than our hybrid method. However, the AC Stark shift in our experiment temporally varies with the power of the write pulse between 16 and 0 MHz which can hardly be compensated for by such stationary two-photon detuning. A stationary two-photon detuning can only ensure that part of the signal pulse is two-photon resonant with the control light while the left part is abandoned. The choice of -9 MHz in our experiment is a compromise for storing most of the signal. Therefore, the best way for high-performance memory is to compensate for the AC Stark shift with a dynamical phase, rather than roughly locking to a stationary detuning.

4.3 Unconditional fidelity

Even storing input signal at the single-photon level, the memory efficiency with the hybrid method can still maintain 87.3% while the traditional intensity method [5] only remains at 83.3%. The improvement in efficiency causes the increase in another criterion, the unconditional fidelity [5,6] $F = |\text{Tr}(\sqrt{\sqrt{\rho_{\text{in}}}\rho_{\text{out}}\sqrt{\rho_{\text{in}}}})|^2$, since the unconditional fidelity is highly sensitive to efficiency. As shown in Figure 7, the fidelity in the hybrid method is 99.0% with an input signal of averaged photon number at 0.4 photon/pulse. Moreover, when the input photons increase, the fidelity of the traditional method [5] drops faster than that of our hybrid method.

As we can see, the fitting shows that the fidelity in traditional one drops below the nonclone limit at averaged photon number of 89.6 photons/pulse. But the hybrid method achieves 59.0% fidelity, outperforms the non-clone limit, and is 8.7% larger than that of the traditional method at the same photon level. Moreover, the fidelity of the hybrid method still outperforms the non-clone limit with an averaged photon number of 128.1 photons/pulse. The maximum photon number of the input state is 42.9% larger than that in the traditional case.

5 Conclusion and discussion

In summary, the phase modulation method has been proven to be useful in optimizing the efficiency of Raman memory. A 13.3% improvement in efficiency was achieved with only phase modulation but poor intensity waveform matching. The hybrid method, which combines intensity and phase modulation, has a total efficiency of up to 87.3%. In comparison to the reported one [5], the hybrid method improves memory efficiency by 5%. Such achievement is because of the elimination of poor intensity waveform

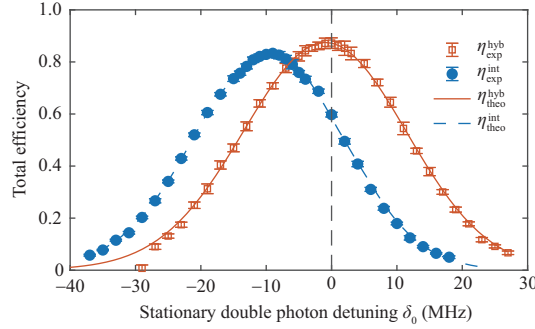


Figure 6 (Color online) Total memory efficiency η as functions of the two-photon detuning. Red squares are for the hybrid method and blue circles are for only the intensity modulation method with the corresponding theoretical simulations (red solid line and the blue dashed line).

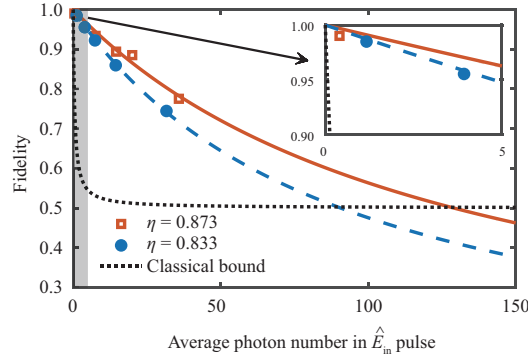


Figure 7 (Color online) The unconditional fidelity as a function of the averaged photon number of the input signal. The red squares are for the hybrid method and blue circles are for only the intensity modulation method with the corresponding fittings (the red solid line and the blue dashed line). The inset is the details in a low photon level.

matching and the suppression of the large dynamic AC Stark shift. Furthermore, a single photon-level experiment shows that the unconditional fidelity is 99.0% with 87.3% memory efficiency. Moreover, unconditional fidelity can outperform the nonclone limit even when the photon number of the input state reaches 128 photons/pulse.

In quantum information processing applications, our method has the advantages of low experimental requirements, an additional degree of freedom, and high performance. The experimental results also show that our system can work well in potential applications involving high speed and high photon number state manipulation. Further improving the performance of Raman memory can still be achieved by improving the atomic density and suppressing the noise, particularly the four-wave mixing (FWM) noise. Benefiting from the energy level and polarization-independent phase modulation method, the FWM noise can be suppressed by combining the hybrid method with noise suppression methods, such as channel blocking [32], cavity [33], and linear absorption [34, 35].

Acknowledgements This work was supported by Innovation Program for Quantum Science and Technology (Grant No. 2021ZD-0303200), Innovation Program of Shanghai Municipal Education Commission (Grant No. 202101070008E00099), National Key Research and Development Program of China (Grant No. 2016YFA0302001), National Natural Science Foundation of China (Grant Nos. 11904227, 12104161, 11654005, 11874152, 12274132, 12204303), Fellowship of China Postdoctoral Science Foundation (Grant Nos. 2020TQ0193, 2021M702146), and Shanghai Municipal Science and Technology Major Project (Grant No. 2019SHZDZX01). Weiping ZHANG also acknowledges additional support from the Shanghai Talent Program.

References

- 1 Ferguson K R, Beavan S E, Longdell J J, et al. Generation of light with multimode time-delayed entanglement using storage in a solid-state spin-wave quantum memory. *Phys Rev Lett*, 2016, 117: 020501
- 2 Bhaskar M K, Riedinger R, Machielse B, et al. Experimental demonstration of memory-enhanced quantum communication. *Nature*, 2020, 580: 60–64
- 3 Heshami K, England D G, Humphreys P C, et al. Quantum memories: emerging applications and recent advances. *J Modern Opt*, 2016, 63: 2005–2028
- 4 Reim K F, Michelberger P, Lee K C, et al. Single-photon-level quantum memory at room temperature. *Phys Rev Lett*, 2011, 107: 053603
- 5 Guo J, Feng X, Yang P, et al. High-performance Raman quantum memory with optimal control in room temperature atoms. *Nat Commun*, 2019, 10: 148

- 6 Hosseini M, Campbell G, Sparkes B M, et al. Unconditional room-temperature quantum memory. *Nat Phys*, 2011, 7: 794–798
- 7 Sparkes B M, Hosseini M, Cairns C, et al. Precision spectral manipulation: a demonstration using a coherent optical memory. *Phys Rev X*, 2012, 2: 021011
- 8 Phillips D F, Fleischhauer A, Mair A, et al. Storage of light in atomic vapor. *Phys Rev Lett*, 2001, 86: 783–786
- 9 Longdell J J, Fraval E, Sellars M J, et al. Stopped light with storage times greater than one second using electromagnetically induced transparency in a solid. *Phys Rev Lett*, 2005, 95: 063601
- 10 Honda K, Akamatsu D, Arikawa M, et al. Storage and retrieval of a squeezed vacuum. *Phys Rev Lett*, 2008, 100: 093601
- 11 de Riedmatten H, Afzelius M, Staudt M U, et al. A solid-state light-matter interface at the single-photon level. *Nature*, 2008, 456: 773–777
- 12 Afzelius M, Simon C, de Riedmatten H, et al. Multimode quantum memory based on atomic frequency combs. *Phys Rev A*, 2009, 79: 052329
- 13 Michelberger P S, Champion T F M, Sprague M R, et al. Interfacing GHz-bandwidth heralded single photons with a warm vapour Raman memory. *New J Phys*, 2015, 17: 043006
- 14 Hsiao Y F, Tsai P J, Chen H S, et al. Highly efficient coherent optical memory based on electromagnetically induced transparency. *Phys Rev Lett*, 2018, 120: 183602
- 15 Ma Y, Ma Y Z, Zhou Z Q, et al. One-hour coherent optical storage in an atomic frequency comb memory. *Nat Commun*, 2021, 12: 2381
- 16 Ding D S, Zhang W, Zhou Z Y, et al. Raman quantum memory of photonic polarized entanglement. *Nat Photon*, 2015, 9: 332–338
- 17 Nunn J, Reim K, Lee K C, et al. Multimode memories in atomic ensembles. *Phys Rev Lett*, 2008, 101: 260502
- 18 England D G, Fisher K A G, MacLean J P W, et al. Storage and retrieval of THz-bandwidth single photons using a room-temperature diamond quantum memory. *Phys Rev Lett*, 2015, 114: 053602
- 19 Gorshkov A V, André A, Lukin M D, et al. Photon storage in λ -type optically dense atomic media. II. Free-space model. *Phys Rev A*, 2007, 76: 033805
- 20 Zhang X, Kalachev A, Kocharovskaya O. All-optical quantum storage based on spatial chirp of the control field. *Phys Rev A*, 2014, 90: 052322
- 21 Minář J, Sangouard N, Afzelius M, et al. Spin-wave storage using chirped control fields in atomic frequency comb-based quantum memory. *Phys Rev A*, 2010, 82: 042309
- 22 Zhang X, Kalachev A, Kocharovskaya O. Quantum storage based on control-field angular scanning. *Phys Rev A*, 2013, 87: 013811
- 23 Kalachev A, Kocharovskaya O. Multimode cavity-assisted quantum storage via continuous phase-matching control. *Phys Rev A*, 2013, 88: 033846
- 24 Dąbrowski M, Chrapkiewicz R, Wasilewski W. Hamiltonian design in readout from room-temperature Raman atomic memory. *Opt Express*, 2014, 22: 26076–26091
- 25 Kalachev A, Kocharovskaya O. Quantum storage via refractive-index control. *Phys Rev A*, 2011, 83: 053849
- 26 Clark J, Heshami K, Simon C. Photonic quantum memory in two-level ensembles based on modulating the refractive index in time: equivalence to gradient echo memory. *Phys Rev A*, 2012, 86: 013833
- 27 Gorshkov A V, André A, Lukin M D, et al. Photon storage in λ -type optically dense atomic media. I. Cavity model. *Phys Rev A*, 2007, 76: 033804
- 28 Shinbrough K, Hunt B D, Lorenz V O. Optimization of broadband λ -type quantum memory using Gaussian pulses. *Phys Rev A*, 2021, 103: 062418
- 29 Appel J, MacRae A, Lvovsky A I. A versatile digital GHz phase lock for external cavity diode lasers. *Meas Sci Technol*, 2009, 20: 055302
- 30 Zahedinejad E, Schirmer S, Sanders B C. Evolutionary algorithms for hard quantum control. *Phys Rev A*, 2014, 90: 032310
- 31 Yang X, Li J, Peng X. An improved differential evolution algorithm for learning high-fidelity quantum controls. *Sci Bull*, 2019, 64: 1402–1408
- 32 Zhang K, Guo J, Chen L Q, et al. Suppression of the four-wave-mixing background noise in a quantum memory retrieval process by channel blocking. *Phys Rev A*, 2014, 90: 033823
- 33 Nunn J, Munns J H D, Thomas S, et al. Theory of noise suppression in λ -type quantum memories by means of a cavity. *Phys Rev A*, 2017, 96: 012338
- 34 Bustard P J, England D G, Heshami K, et al. Reducing noise in a Raman quantum memory. *Opt Lett*, 2016, 41: 5055–5058
- 35 Thomas S E, Hird T M, Munns J H D, et al. Raman quantum memory with built-in suppression of four-wave-mixing noise. *Phys Rev A*, 2019, 100: 033801

Appendix A

According to [19], the equations for the Raman memory with dynamic two-photon detuning are

$$\left(c \frac{\partial}{\partial z} + \frac{\partial}{\partial t}\right) \hat{E}(z, t) = ig\sqrt{N}\hat{P}, \quad (\text{A1})$$

$$\frac{\partial}{\partial t} \hat{P}(z, t) = -(\gamma + i\Delta_s)\hat{P} + ig\sqrt{N}\hat{E} + i\Omega\hat{S}, \quad (\text{A2})$$

$$\frac{\partial}{\partial t} \hat{S}(z, t) = i(\Delta_c - \Delta_s)\hat{S} + i\Omega^*\hat{P}, \quad (\text{A3})$$

where $\hat{E}(z, t)$, $\hat{P}(z, t)$, $\hat{S}(z, t)$ are the slowly varying envelope operators of the signal field, atomic polarization σ_{ge} , and atomic spin wave $\sigma_{gm}e^{i(\Delta_c - \Delta_s)t}$, respectively, the atomic operators $\sigma_{ij} = |i\rangle\langle j|$ ($i, j = g, e, m$). Here we introduce the polarization decay rate γ , but neglect the Langevin force operators under reasonable experimental conditions [19]. With large detuning $\Delta \gg \gamma, \Omega$, we can neglect the small decay rate γ and do the adiabatic approximation of the polarization equation as $\frac{\partial}{\partial t} \hat{P}(z, t) = 0$ which gives

$$\left(c \frac{\partial}{\partial z} + \frac{\partial}{\partial t}\right) \hat{E}(z, t) = i\tilde{\kappa}(t)\hat{S}, \quad (\text{A4})$$

$$\frac{\partial}{\partial t} \hat{S}(z, t) = -i\tilde{\delta}(t)\hat{S} + i\tilde{\kappa}^*(t)\hat{E}. \quad (\text{A5})$$

Here we neglect the dispersion part $g^2 N \hat{E} / \Delta_s$. By integrating on z direction we can neglect the propagation effect. Let

$$\int_0^L \hat{E}(z, t) dz = \hat{A}(t), \quad \int_0^L \hat{S}(z, t) dz = \hat{B}(t), \quad (\text{A6})$$

where

$$\int_0^L \frac{\partial}{\partial z} \hat{E}(z, t) dz = \hat{E}_{\text{out}}(t) - \hat{E}_{\text{in}}(t). \quad (\text{A7})$$

Absorbing a factor \sqrt{c} into the definition of $\hat{E}(t)$ and $\hat{\kappa}(t)$, the equations become

$$\frac{d}{dt} \hat{A}(t) = i\hat{\kappa}(t)\hat{B} + \hat{E}_{\text{in}}(t) - \hat{E}_{\text{out}}(t), \quad (\text{A8})$$

$$\frac{d}{dt} \hat{B}(t) = -i\hat{\delta}(t)\hat{B} + i\hat{\kappa}^*(t)\hat{A}. \quad (\text{A9})$$

Appendix B

In the memory process, the output signal E_{out} at the end of the cell depends on the input signal, intensity, and phase waveform of the control field. The expression of the output signal can be solved from (A4) and (A5) with the Laplace transform method [27]¹⁾ as

$$\hat{E}_{\text{out}}(t) \approx \hat{E}_{\text{in}}(t) - \sqrt{L}\kappa(L, t) \int_0^\tau \hat{E}_{\text{in}}(\tau') \kappa^*(\tau') D(\tau, \tau') \frac{J_1[2\sqrt{zp(\tau, \tau')}]}{\sqrt{p(\tau, \tau')}} d\tau', \quad (\text{B1})$$

where $D(\tau, \tau') = \exp[-i \int_{\tau'}^\tau \hat{\delta}(\tau'') d\tau'']$, $p(\tau, \tau') = \int_{\tau'}^\tau |\hat{\kappa}(\tau'')|^2 d\tau''$, $\tau = t - z/c$, $\tau' = t' - z'/c$, $\tau'' = t'' - z''/c$ are the co-moving coordinates. As we can see, the expression of \hat{E}_{out} is a nonlinear one. But in the optimal situation, the memory process transforms almost all the signal into a spin wave which makes the output signal small. So in the discussion of optimization, we can approximately set $\hat{E}_{\text{out}} \rightarrow 0$ which makes our discussion easy and reasonable.

1) Raymer M G, Mostowski J. Stimulated Raman scattering: unified treatment of spontaneous initiation and spatial propagation. *Phys Rev A*, 1981, 24: 1980–1993.